J. Fluid Mech. (1988), *vol.* 193 *pp.* 267–283
Printed in Great Britain

Peristaltic pumping in circular cylindrical tubes: a numerical study of fluid transport and its efficiency

By S. TAKABATAKE,† K. AYUKAWA† AND A. MORI‡

† Department of Mechanical Engineering, Ehime University, Bunkyo-cho, Matsuyama, Ehime 790, Japan

‡ Mitsubishi Heavy Industry Co. Ltd., Mihara Works, Itozaki-cho, Mihara, Hiroshima 723, Japan

(Received 26 March 1987 and in revised form 29 October 1987)

A numerical method employing an upwind finite-difference technique is adopted for an investigation of peristaltic pumping in circular cylindrical tubes, such as some organs in the living body. Various peristaltic flows are calculated under conditions of finite wave amplitudes, finite wavelengths and finite Reynolds numbers, and the influence of the magnitude of these quantities on the flow is investigated. The fluid mechanics of peristaltic mixing and transport are studied in detail by analysing the reflux and the trapping phenomena. The mechanical efficiency of peristaltic pumping is also discussed, with reference to engineering and physiological applications. It is shown that quantitative differences are observed between the results obtained for flows in a circular cylindrical tube and a two-dimensional plane channel. However, for both cases the appearance of peristaltic reflux depends upon the Reynolds number and the wavenumber (mean tube radius/wavelength). Much greater peristaltic mixing and transport are realized in a circular tube than in a plane channel.

1. Introduction

Peristaltic pumping is well known as a form of fluid transport that is used by many systems in the living body to propel or to mix the contents of a tube. In 1969, Shapiro, Jaffrin & Weinberg investigated the fluid mechanics of peristaltic pumping in connection with the function of systems such as the ureter, the gastro-intestinal tract, the small blood vessels, and other glandular ducts. They found that there were two physiologically significant phenomena called 'reflux' and 'trapping' in peristaltic flow. The former refers to the net retrograde motion of some part of the fluid in a direction opposite to the wave propagation on the wall. The latter means the development and transport of an internally circulating bolus of fluid.

The mechanism of this mixing and transporting peristaltic motion has aroused general interest in the field of hydrodynamics, and a number of studies have been done to understand peristaltic motion in different situations. The early literature has been reviewed by Jaffrin & Shapiro (1971). The results of some of the theoretical investigations are summarized in table 1, arranged according to the flow geometry and the following parameters of the problem:

$$\text{amplitude ratio} \quad \phi = \epsilon/h; \tag{1}$$

$$\text{wavenumber} \quad \alpha = h/\lambda; \tag{2}$$

$$\text{Reynolds number} \quad R_e = (ch/\nu)\alpha; \tag{3}$$

Author(s)	Geometry	R_e	α	ϕ	Other restrictions
Shapiro, Jaffrin & Weinberg (1969)	P, A	0	0	arb.	
Pozrikidis (1987)	P	0	arb.	arb.	
Jaffrin (1973)	P	small	small	arb.	
Zien & Ostrach (1970)	P	small	small	arb.	zero mean flow
Li (1970)	A	small	small	arb.	zero mean flow
Manton (1975)	A	small	small	arb.	
Liron (1976)	P, A	small	small	arb.	
Fung & Yih (1968)	P	arb.	arb.	small	$\phi R_e \alpha \ll 1$
Yin & Fung (1969)	A	arb.	arb.	small	$\phi R_e \alpha \ll 1$
Hanin (1968)	P	arb.	0	small	zero mean pressure gradient
Longuet-Higgins (1983)	P	arb.	small	small	
Ayukawa, Kawai & Kimura (1981)	P	high	small	small	

TABLE 1. Summary of theoretical investigations. P, plane channel; A, axisymmetric tube.

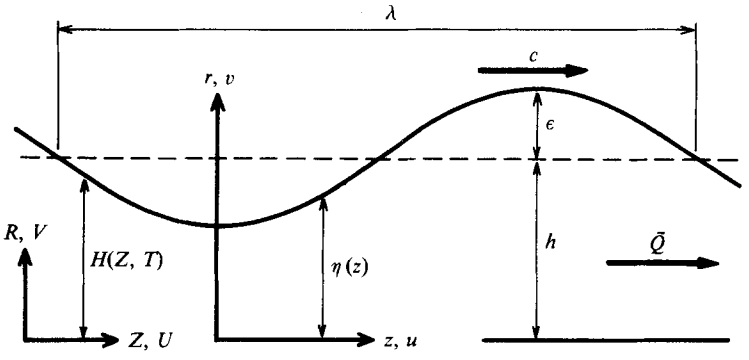

FIGURE 1. Geometry of axisymmetric tube and travelling wave system.

where ϵ, λ and c are the wave amplitude, the wavelength and the wave speed respectively, h is the mean tube radius and ν is the kinematic viscosity (see figure 1). Besides these investigations, there are many analyses of other similar topics, such as the interaction of the elastic wall and the fluid (Rath 1978), the effect of a non-uniform tube (Gupta & Seshadri 1976), the effect of a non-Newtonian fluid (Böhme & Friedrich 1983), and the effect of a peripheral layer (Srivastava & Srivastava 1984 and Brasseur, Corrsin & Lu 1987). Most of these studies have been made under certain simplifying assumptions regarding the magnitudes of the wave amplitude, the wavelength, the Reynolds number and the time-mean flow, and the general approach has been to employ asymptotic expansions of one kind or another in the parameters ϕ, α and R_e. Therefore, although these analyses give us the main feature of peristaltic pumping at small values of these parameters, they are not sufficient to describe the mechanisms of the flow for general conditions. On the other hand, a few numerical investigations have also been reported. Tong & Vawter (1972) obtained finite-element solutions in the limit of creeping motion. Brown & Hung (1977) used the finite-difference method in a study concerned with nonlinear flow at finite Reynolds numbers. Takabatake & Ayukawa (1982, hereinafter referred to as T & A) also presented finite-difference solutions for two-dimensional peristaltic flows.

It is the purpose of the present paper to solve the problem of peristaltic pumping in an axisymmetric tube by generalizing the numerical method of T & A to the axisymmetric case. It has now been accepted that the cases of a two-dimensional channel and an axisymmetric tube yield qualitatively similar results. But, since glandular ducts and other tracts of the body involving peristalsis are approximately cylindrical in shape and the flow seems to be somewhat more axisymmetric than two-dimensional, the axisymmetric case would probably be more realistic physiologically. There is also merit in studying the axisymmetric case to identify differences between the two cases. In this paper a numerical investigation of the influence of the magnitudes of wave amplitude, wavelength, Reynolds number, and time-mean flow on an axisymmetric peristaltic flow is conducted. In particular, the fluid mechanics of peristaltic mixing and transport are studied in detail by analysing the reflux and the trapping phenomena. From a comparison of these results with those for the two-dimensional plane case, the quantitative difference between both cases is evaluated.

In addition, the mechanical efficiency of peristaltic pumping is analysed in this paper. In regard to efficiency, Shapiro *et al.* (1969) conducted a primary study for the limiting flow of infinite wavelength and zero Reynolds number. However, these authors discovered that they made a calculated mistake in reducing the efficiency expression in the axisymmetric case and this error seems to have been left uncorrected. The correct expression for the efficiency is presented in Appendix B, and the pumping characteristics are discussed through numerical calculations over a wide parameter range for both the axisymmetric- and the two-dimensional-flow cases.

Our analysis has the following limitation. Although the theoretical analyses in previous works have been limited in scope, the present numerical method has no restriction, in principle. But, as is usual with numerical analyses, there is the parametric restriction resulting from convergence failure. The calculations at large Reynolds number have failed to converge in the range of small time-mean flow, and our results in this range are thus limited.

2. Description of the numerical analysis

The numerical method used here is based on that developed for the two-dimensional plane channel in the earlier papers by T & A and Ayukawa & Takabatake (1982). The concepts and procedures for the axisymmetric case are identical with those for the plane case, although the details of the calculation are more complicated. Thus, we present here only an outline of the numerical method. The terminology in the present paper is the same as that in T & A, unless otherwise stated.

The fluid is assumed to be Newtonian, viscous, homogeneous, and incompressible. An axisymmetric tube with longitudinal Z-axis and radial R-axis is considered (see figure 1). An infinite train of sinusoidal waves progresses along the wall with velocity c. In the wave-fixed relative frame (with local coordinates z, r and velocity components u, v), i.e. the wave frame, the flow in the tube is steady. Therefore, we shall largely base our analysis on this reference frame, and the flow in the laboratory frame (with coordinates Z, R and velocity components U, V) will be derived from this steady solution.

The flow induced by an infinite train of peristaltic waves is expected to be the same as a periodic flow that is independent of the boundary conditions at the end sections. We therefore consider a finite region with an integral number of waves in the wave frame. The boundary conditions are arbitrary conditions on the two end sections, the symmetry condition on the centre axis, and the no-slip condition on the wall.

The Navier–Stokes equations are reduced to the vorticity transport equation, involving the vorticity ω and the Stokes stream function ψ. The new variable ζ, defined by $\zeta = r\omega$ (r being the radial coordinate), is introduced to simplify the discussion of the numerical method. Then we use a finite-difference technique to solve the problem in terms of ψ and ζ in a finite calculation region, together with the boundary conditions mentioned above.

The finite-difference expressions for the governing equations are derived by applying the well-known, first-order-accurate, upwind difference technique established by Greenspan (1968). Namely, an upwind difference approximation is used for the convective terms of the vorticity transport equation, while the diffusive terms are approximated by using centred differences. The finite-difference formulation and the computational procedure are very similar to that in T & A. In Appendix A we show a representative group of the resulting difference expressions. The successive-over-relaxation (SOR) method is used to solve them. In the present calculation the convergence criteria for the numerical solutions are chosen as $r\epsilon_\psi$ for ψ and $r\epsilon_\omega$ for ζ, while the criteria ϵ_ψ for ψ and ϵ_ω for ω were used in the two-dimensional analysis by T & A. Thus, the accuracy of the velocity and vorticity fields determined in the present calculation is uniform over the entire flow field, just as in the two-dimensional analysis.

3. Results and discussion

The problem of peristaltic pumping is governed by four dimensionless parameters: the amplitude ratio ϕ, the wavenumber α, the Reynolds number R_e, and the dimensionless time-mean flow $\bar{\mathcal{Q}}$. The first three have been defined in (1)–(3) and are the same definitions used in T & A. The dimensionless time-mean flow is here defined by

$$\bar{\mathcal{Q}} = \bar{Q}/\pi c h^2, \tag{4}$$

where $\bar{Q}$ is the time-mean rate of volume flow. In T & A this quantity was defined as $\bar{\mathcal{Q}} = \bar{Q}/ch$. Thus, the parameter $\bar{\mathcal{Q}}$ indicates the dimensionless mean-volume flow per unit area for both the tubular and planar cases, whereas the cross-sectional shapes are quite different. There are several definitions of the Reynolds number in the literature, but the one used here has been shown to be the correct ratio of inertial and viscous terms when peristalsis acts as a pump (Shapiro *et al.* 1969). It should be noted that this definition of the Reynolds number also characterizes the ratio of the radial vorticity diffusion time to the period of the wave.

In the present calculations, the mesh limits N and M, the relaxation factors ξ_ψ and ξ_ω, and the weight factors δ_ψ and δ_ω have the values $N = M = 30$, $\xi_\psi = 1.8$, $\xi_\omega = 0.8$, $\delta_\psi = 0.1$ and $\delta_\omega = 0.8$, consistent with those in T & A. The tolerances ϵ_ψ and ϵ_ω used in the iteration processes are taken to be $\epsilon_\psi = 10^{-5}$ and $\epsilon_\omega = 2 \times 10^{-4}$. Among these quantities, N, M, ϵ_ψ and ϵ_ω relate to the accuracy of the numerical solution, while ξ_ψ, ξ_ω, δ_ψ and δ_ω determine the convergence and the stability of calculations.

The validity of the present analysis has been confirmed by the fact that the calculated velocity profiles for $R_e = 0.01$ and $\alpha = 0.01$ agree within one percent with the theory of inertia-free, long-wavelength flow ($R_e \to 0$, $\alpha \to 0$) developed by Shapiro *et al.* (1969). In addition, the numerical accuracy at moderate values of R_e and α is also judged to be satisfactory through a detailed investigation of particle trajectories (§3.1).

Calculations are performed for the various flows over a wide range of Reynolds

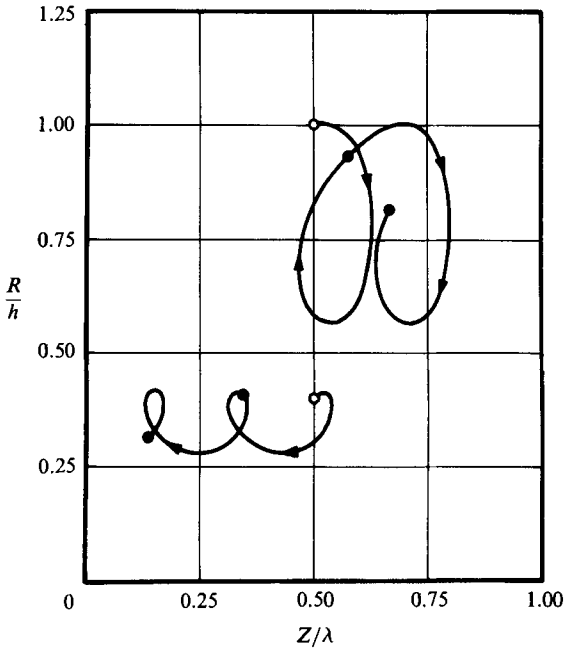

FIGURE 2. Examples of particle trajectories; $\phi = 0.25$, $\alpha = 0.2$, $R_e = 10$, $\bar{Q} = 0$. ○, initial locations; ●, locations at the end of one and two wave periods.

numbers, wavenumbers, amplitude ratios, and time-mean flow rates. In the following sections, representative results of these computations are presented, and arguments about the mixing and the transport mechanisms and the mechanical efficiency of peristalsis are developed.

3.1. *Peristaltic reflux*

The 'peristaltic reflux' was defined for phenomena such as the retrograde motion of bacteria from the bladder to the kidneys. In order to ascertain the presence of the reflux, it is necessary to examine Lagrangian trajectories of individual fluid particles and to determine whether there are any particles undergoing net negative displacement.

The trajectory of a particle can be obtained by integrating the simultaneous equations

$$\frac{dZ}{dT} = U, \quad \frac{dR}{dT} = V \tag{5}$$

successively from the initial location of the particle. The integration is carried out numerically by the Runge–Kutta method.

Examples of the particle trajectories at moderate Reynolds number are illustrated in figure 2, in which the open circles indicate the initial locations and the filled circles show the locations at the end of one and two wave periods.

Figure 2 demonstrates that the axisymmetric tube and the two-dimensional plane channel flows yield qualitatively similar results for the motion of fluid particles. Although the individual particles in the flow repeat the same trajectories periodically, they do not describe exactly closed paths, and their orbital motions possess net longitudinal displacements. Moreover, the resultant particle period T_p, which is

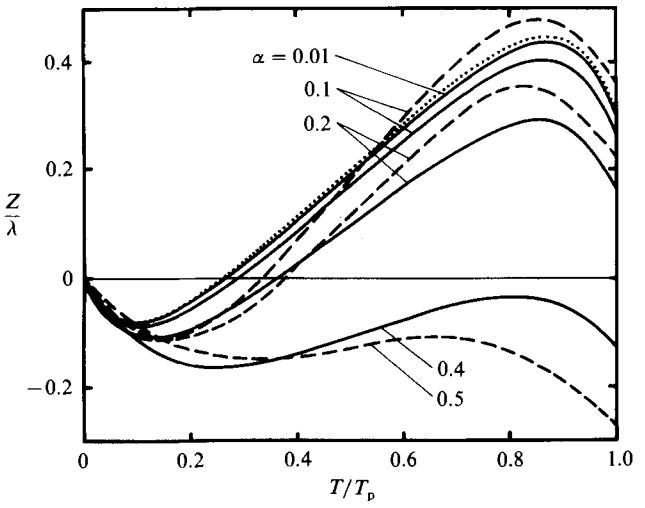

FIGURE 3. Trajectories of fluid particles on the axis for $\phi = 0.25$, $\bar{\mathcal{Q}} = 0$. ——, Present method for $R_e = 0.01$; ·····, Shapiro *et al.* (1969) for $R_e \to 0$, $\alpha \to 0$; – – –, Tong & Vawter (1972) for $R_e \to 0$.

R_e	α	Present D/λ, T_p/T_w	Shapiro *et al.* D/λ, T_p/T_w	Tong & Vawter D/λ, T_p/T_w
0.01	0.01	0.292 1.290	0.306 1.306	—
	0.1	0.262 1.265	—	0.36 1.44
	0.2	0.164 1.165	—	0.22 1.32
	0.4	−0.128 0.871	—	—
	0.5	—	—	−0.27 0.83
1 10	0.2	0.109 1.108 −0.256 0.745	—	—

TABLE 2. Particle periods and net longitudinal displacements for particle motions on the axis; $\phi = 0.25$, $\bar{\mathcal{Q}} = 0$

defined as the time interval of one orbital motion, does not always coincide with the wave period T_w. These interesting conclusions are identical with those obtained in the two-dimensional flow study; see T & A.

Figure 3 shows the motions of fluid particles on the axis in the case of zero time-mean flow. In this figure, the present results for $R_e = 0.01$ are compared with the solution of Shapiro *et al.* (1969) obtained in the limit $R_e \to 0$, $\alpha \to 0$, and with the numerical results of Tong & Vawter (1972) employing a finite-element method for the limit $R_e \to 0$. Each fluid particle initially ($T = 0$) positioned at the trough section of

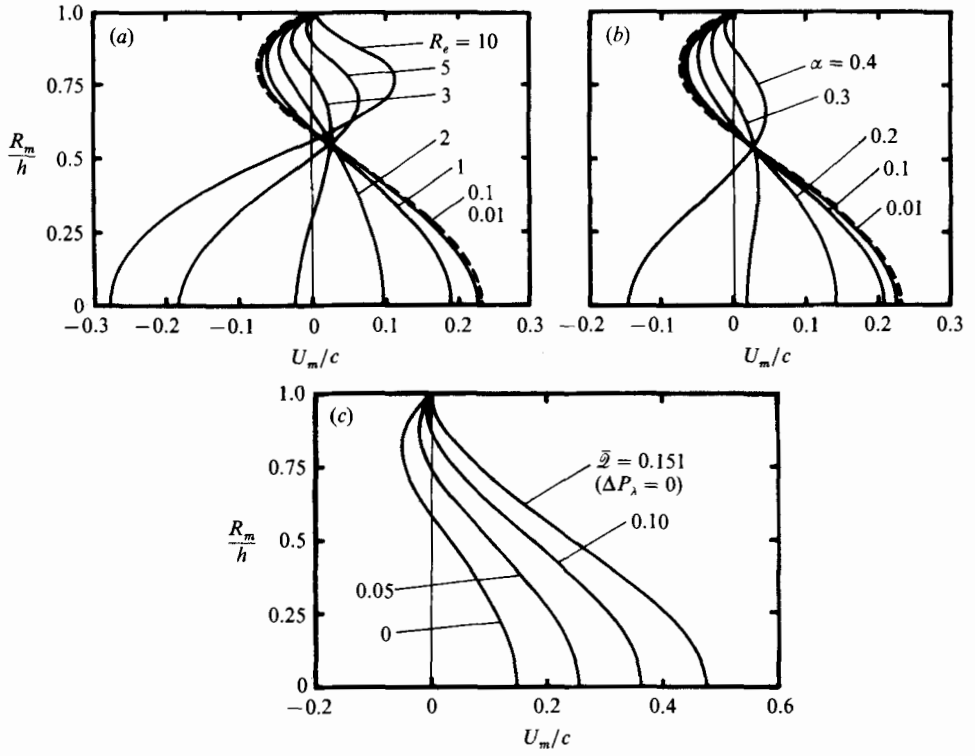

FIGURE 4. Curves of mass transport velocity for the fluid particles, plotted against the mean lateral position of the particle trajectory. (*a*) $\phi = 0.25$, $\alpha = 0.01$, $\bar{Q} = 0$; (*b*) $\phi = 0.25$, $R_e = 0.01$, $\bar{Q} = 0$; (*c*) $\phi = 0.2$, $\alpha = 0.01$, $R_e = 0.01$. ——, Present; – – –, Shapiro *et al.* (1969).

the wave undergoes first a backward motion followed by a forward one, then a backward one again, as time progresses. At the end of each particle period ($T = T_p$), the particle experiences a net positive longitudinal displacement for small α, while it undergoes a net negative longitudinal displacement for large α. The latter shows the presence of the reflux.

In our results, shown by solid curves, the $\alpha = 0.01$ case is in excellent agreement with the theory of Shapiro *et al.* On the other hand, the results by Tong & Vawter show that the displacements during both the backward and the forward motion are greater than our estimations, and, therefore, their particle trajectories differ from those obtained in the present study and in the study of Shapiro *et al.*

Table 2 shows numerical results for the particle period T_p/T_w and the net longitudinal displacement D/λ during one particle period for particle motions on the axis, together with those obtained by other analyses. Shapiro *et al.* reported that the relationship between D/λ and T_p/T_w was represented by

$$D/\lambda = T_p/T_w - 1. \tag{6}$$

This relationship has to hold not only in the limit $R_e \to 0$, $\alpha \to 0$, but also under the conditions of finite values of R_e and α, in order that the fluid particles should repeat the same trajectories. It can be seen that the present results satisfy this relationship very well even for moderate values of R_e and α. Thus, although a direct comparison of our solution with those of other analyses is unattainable in the range of finite Reynolds number and wavenumber, it may be concluded that the numerical method

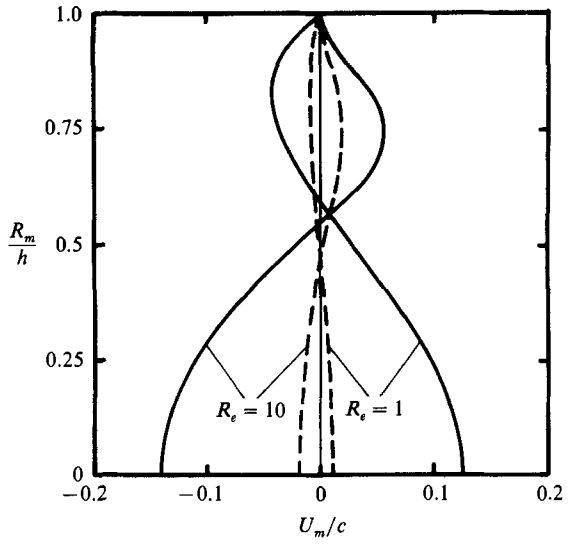

FIGURE 5. Profiles of mass transport velocity for $\phi = 0.2$, $\alpha = 0.01$, $\bar{Q} = 0$. ——, For axisymmetric tube; – – –, for two-dimensional channel.

described in this paper produces realistic solutions for finite Reynolds numbers and finite wavenumbers.

The dependences of the radial profile of the mass transport velocity on R_e, α and $\bar{Q}$ are shown in figure 4. It was first shown by Stokes (1847) that in a water wave the particles of fluid possess steady second-order drift velocities, apart from their orbital motions. This mean velocity is usually called the mass transport velocity. The mass transport velocity U_m in peristaltic flow can be obtained from

$$U_m = D/T_p. \tag{7}$$

We may ascertain the presence of reflux when there is a region in a tube where U_m is negative. It is seen in the figure that U_m is negative in the region near the wall of the tube and is positive in the region near the axis when both R_e and α are small, for small values of $\bar{Q}$. For this situation, Shapiro *et al.* concluded that reflux occurred near the wall of the tube. But figure 4 indicates that the location of the reflux phenomenon in the flow depends upon the magnitudes of R_e and α. That is, reflux takes place near the axis for large Reynolds number and/or for large wavenumber, whereas it occurs near the wall for small R_e and small α as pointed out by Shapiro *et al.* The motion of a fluid particle depends on the Eulerian velocity distribution in the tube. When $R_e = 0$ and $\alpha = 0$, the profiles of the longitudinal component of velocity are locally Poiseuille-like, and all radial components vanish. However, when R_e and α are large the profiles deviate from the parabolic profile due to the effects of fluid inertia and wall slope (see T & A). This difference in the velocity field causes the different behaviour of a fluid particle according to whether the Reynolds number and/or the wavenumber are small or large.

Although this interesting result with respect to the appearance of reflux is essentially identical with that for the two-dimensional case, there is a quantitative difference between the magnitudes of the mass transport velocities in the two cases. A comparison between them is made in figure 5, which shows that the magnitudes of the mass transport velocities in the axisymmetric case are a factor of ten greater

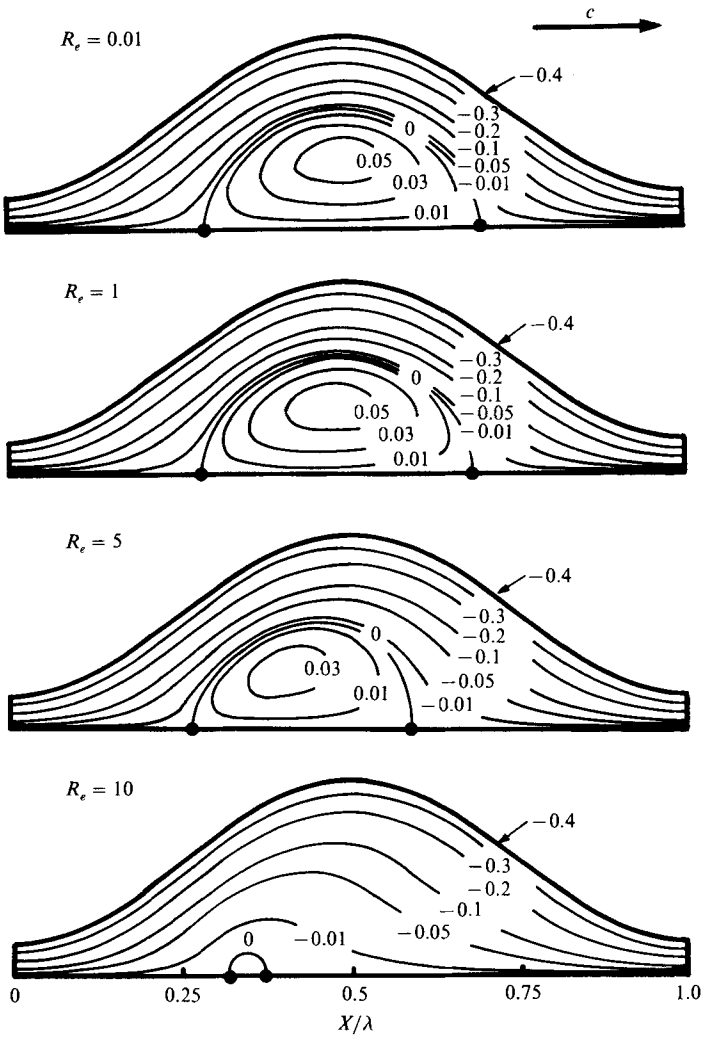

FIGURE 6. Wave-frame streamlines in a two-dimensional flow for $\phi = 0.7$, $\alpha = 0.01$, $\bar{\mathcal{Q}} = 0.6$.

than those in the two-dimensional case. Thus it may be concluded that the reflux phenomenon is much stronger in a circular tube than in a two-dimensional channel. In other words, peristalsis in a tubular configuration results in a strong mixing flow compared with that in a two-dimensional plane configuration.

3.2. *Trapping phenomenon*

It has been observed that for certain values of ϕ and $\bar{\mathcal{Q}}$ a part of the fluid in the tube is enclosed by a streamline separated from the axis in the wave frame and is transported with a wave speed in the laboratory frame as if it were trapped by the wave. Examples of this interesting phenomenon called 'trapping' are shown in figure 6 for a two-dimensional flow and in figure 7 for an axisymmetric flow. In these figures, the computational flow patterns observed in the wave frame are illustrated for various flows over a wide range of Reynolds numbers.

It might be interesting to compare quantitatively these characteristics in the two

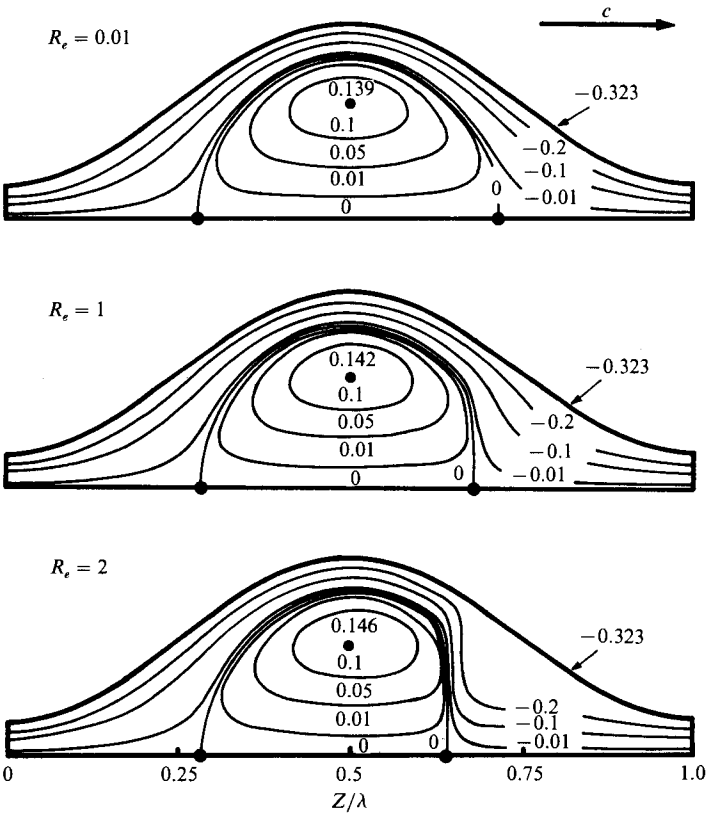

FIGURE 7. Wave-frame streamlines in an axisymmetric flow for $\phi = 0.7$, $\alpha = 0.01$, $\bar{\mathcal{Q}} = 0.6$.

cases. The choice of the appropriate parameter for comparing these flows must be made with caution because the geometrical cross-sections are different. However, since we make a comparison for the same values of $\bar{\mathcal{Q}}$, as well as the same ϕ and α, both the dimensionless mean volume flows per unit area and the linear dimensions of geometrical shape are the same in both cases. The comparison developed here may therefore provide useful insight toward understanding the quantitative differences of flow characteristics between the tubular and planar cases.

In the case of the two-dimensional flow of figure 6, as the Reynolds number increases, the trapping becomes gradually smaller and moves backward, owing to the backward flow from the narrowest region of the channel. Trapping ceases to exist when the Reynolds number becomes sufficiently large. However, in axisymmetric flow, as shown in figure 7, although the front part of the trapping is seen to be broken off, the major part does not change shape and the trapping does not move. In addition, the maximum magnitude of the stream function in the trapping is kept nearly constant when the Reynolds number is increased.

Jaffrin (1973) studied theoretically the effect of small fluid inertia on the trapping phenomenon in a two-dimensional channel flow, and found that the inertial effect restrains the appearance of trapping. But he did not refer to the detailed flow pattern when the trapping occurred at finite Reynolds number. Figures 6 and 7 present this situation for both the two-dimensional and axisymmetric flow cases and support the conclusion of Jaffrin.

The flow patterns illustrated in figure 7 are very informative. As the Reynolds

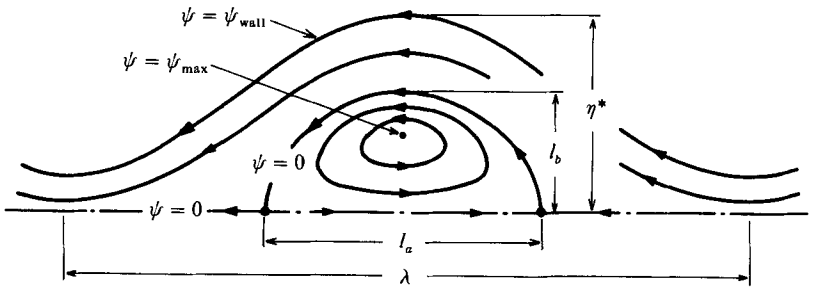

FIGURE 8. Definition sketch of the trapping.

number increases, the streamlines at the right-hand side are deflected away from the wall, suggesting a flow separation and the formation of the second free eddy. But we did not observe the closed streamlines in this region for the flow up to $R_e = 2$. Our calculation encountered convergence failure for further increases in the Reynolds number. It is possible that the convergence failure might result from the complication of the flow due to the appearance of the second eddy.

In order to discuss the appearance and growth of the trapping in detail, we define certain quantities in figure 8. The dimensions of the trapping l_a and l_b may be measured by the longitudinal and lateral length of the trapped-fluid region enclosed by the split streamline. These quantities are normalized with respect to the wavelength λ and the maximum tube radius η^*, respectively. Also, the relative intensity of the trapping may be characterized by the ratio of the maximum magnitude of the stream function within the trapped region ψ_{max} to the magnitude of the stream function along the tube wall ψ_{wall}.

The effects of Reynolds number on the trapping lengths l_a and l_b and on the trapping intensity $|\psi_{max}/\psi_{wall}|$ are presented in figure 9. The results for axisymmetric flow, shown by the solid curves, are compared with those for two-dimensional flow, the dashed curves. In these figures, the value of $\bar{Q}$ at the left end of each curve expresses the lower limit of the time-mean flow at the first appearance of the trapping, and the value at the right end gives the maximum time-mean flow transported by the peristaltic pumping, that is, when no pressure difference is imposed along the tube. However, because the calculations for the axisymmetric case at $R_e > 2$ failed to converge in the range of small time-mean flow, our results in this range are limited.

In both the axisymmetric- and two-dimensional-flow cases, the curves of l_a and l_b shift toward the right and their slopes become steeper as R_e increases. It is evident from this fact that the time-mean flow for the trapping limit increases as the Reynolds number increases. In addition, the trapping at large Reynolds numbers can grow suddenly as the result of a slight increase in the time-mean flow, in contrast to that at small Reynolds numbers. In figure 9(*c*), which shows the trapping intensity, it is seen that the intensities for the axisymmetric case are almost twenty times as large as those for the two-dimensional case, and the dependence of the intensity on Reynolds number is less evident in the former case than in the latter. Thus, it is concluded that the dimension and the intensity of the trapping are less sensitive to an increase in Reynolds number in axisymmetric flow than in two-dimensional flow. The convective transport of fluid by means of the trapping phenomenon in a circular cylindrical tube can therefore take place actively within a wider range of Reynolds numbers than in a two-dimensional plane channel.

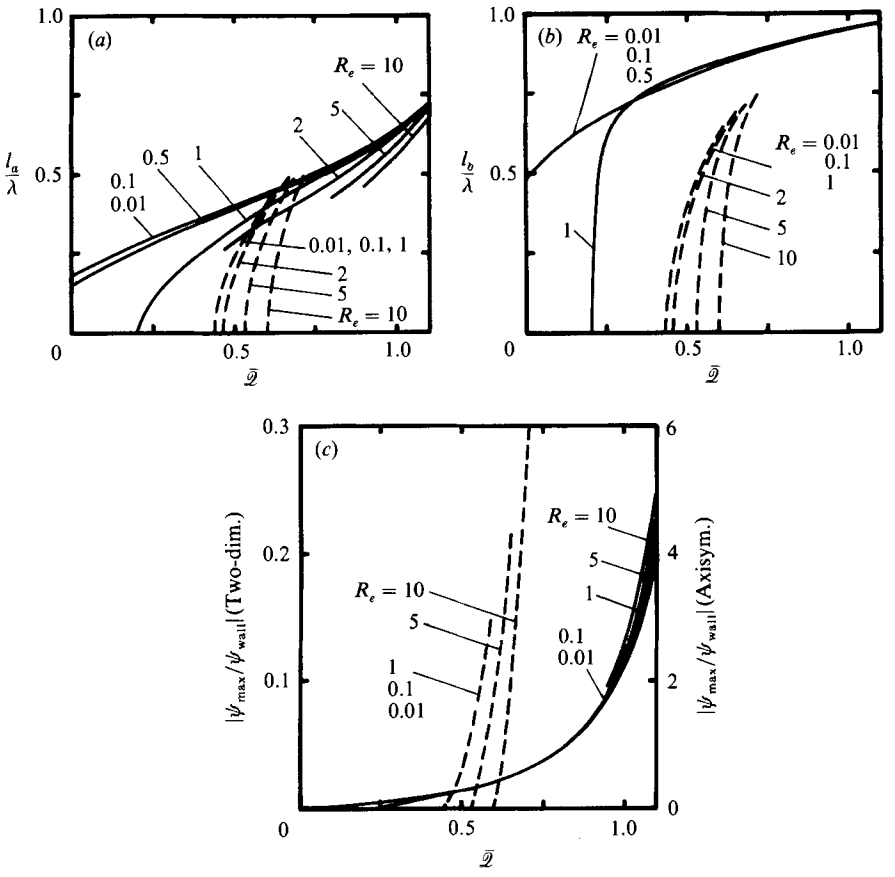

FIGURE 9. Effects of Reynolds number on the trapping phenomenon; $\phi = 0.7$, $\alpha = 0.01$. (*a*) Longitudinal length; (*b*) lateral length; (*c*) relative intensity. ——, Axisymmetric flow; – – –, two-dimensional flow.

3.3. *Pumping efficiency*

The mechanical efficiency of peristaltic pumping is defined as the ratio of the useful energy W_W stored in the fluid to the mechanical work W_L delivered to the wall from outside agencies, and is given by Shapiro *et al.* (1969) as

$$\eta_t = \frac{W_W}{W_L} = \frac{\bar{Q}\Delta P_\lambda}{-\frac{1}{T_w}\int_0^{T_w}\int_0^{\lambda} 2\pi H v(p - \sigma_r + \tau_{zr}\tan\theta)\,\mathrm{d}Z\,\mathrm{d}T}, \tag{8}$$

where ΔP_λ is the pressure rise per wavelength and $\tan\theta$ denotes the wall slope. H, v, p, σ_r, τ_{zr} and $\tan\theta$ represent the instantaneous values at the point on the wall. These values as well as $\bar{Q}$ and ΔP_λ will be calculated numerically, in the manner developed in T & A.

Shapiro *et al.* (1969) obtained the linear solution for peristaltic flows by considering the limiting case of $R_e \to 0$, $\alpha \to 0$, for both the axisymmetric and two-dimensional plane geometries. For $\alpha \to 0$, the contribution of the viscous stress terms to the mechanical-work integral in (8) can be negligible compared with that of the pressure

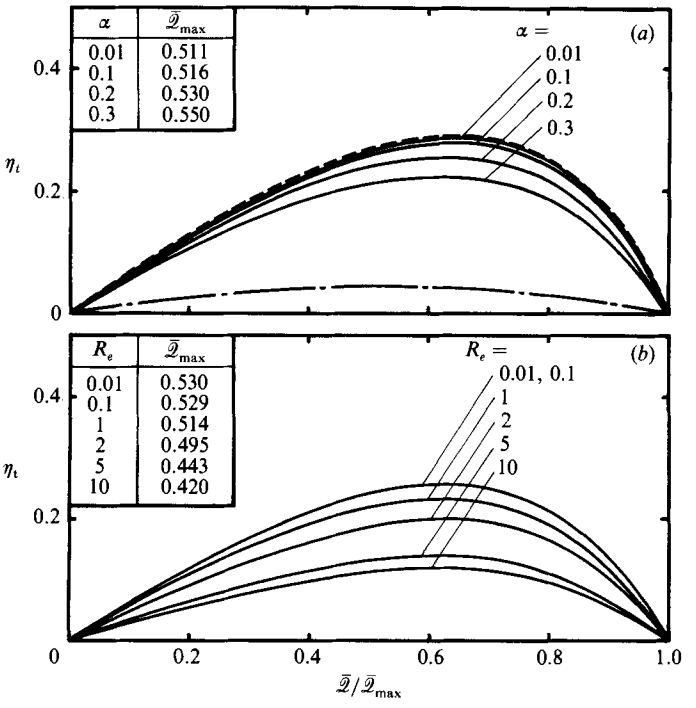

FIGURE 10. Pumping efficiencies for axisymmetric case. (*a*) $\phi = 0.4$, $R_e = 0.01$; (*b*) $\phi = 0.4$, $\alpha = 0.2$. ——, Present; – – –, linear solution; —·—, Shapiro *et al.* (1969).

term. Thus they obtained a simple expression for the efficiency η_t by neglecting the contributions of σ_r and τ_{zr} and by solving the linear flow problem. The calculated efficiencies were compared with those for the plane case and the results showed that the efficiency is much smaller in an axisymmetric configuration than in a plane configuration; see figure 4 of Shapiro *et al.* (1969). But the present authors have discovered that the efficiency expression for the axisymmetric case obtained by Shapiro *et al.* is incorrect. They made an error in evaluating the integral of (8). In Appendix B, the correct expression for the efficiency for the limiting case $R_e \to 0$, $\alpha \to 0$ is derived by the authors on the basis of the analysis of Shapiro *et al.* and shall be called hereafter the solution of the linear analysis.

The effects of ϕ, α, R_e and $\bar{Q}$ on the pumping efficiency η_t are presented in figure 10, together with the linear solution and the solution of Shapiro *et al.* In the figures, the ratio of the time-mean flow $\bar{Q}$ to the maximum time-mean flow $\bar{Q}_{max}$ (for $\Delta P_\lambda = 0$) is the abscissa. The numerical result for $R_e = 0.01$ and $\alpha = 0.01$ is in excellent agreement with the linear solution. As shown in figure 10(*a*), η_t decreases with increasing α. In the range of large α, useful mechanical energy cannot be stored in the fluid because large viscous dissipation is produced in the whole region of the flow due to the large curvatures of the streamlines. Therefore it is thought that the efficiency decreases with increasing α. Figure 10(*b*) shows that the efficiency also decreases with increasing R_e. It has been previously reported (T & A; Takabatake, Ayukawa & Okura 1985) that in the case of large R_e the work done by the motion of the wall is mainly cancelled between the dilating part and the contracting part and the useful energy is not stored in the fluid, while for small R_e the flow receives energy equal to

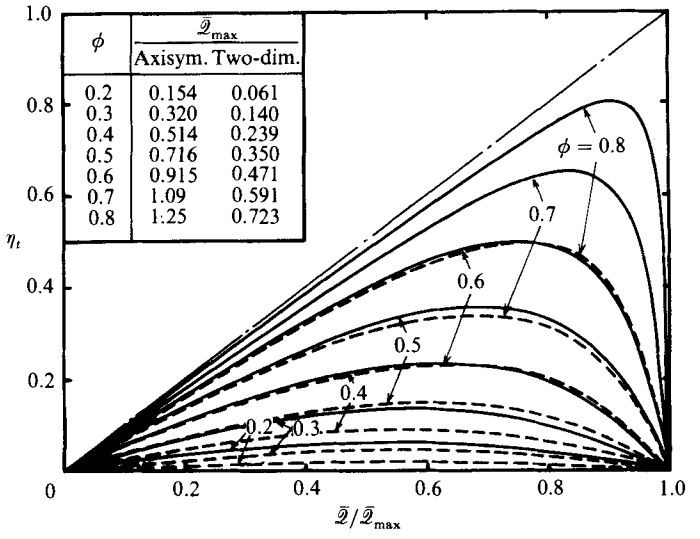

FIGURE 11. Comparison between the efficiencies of the axisymmetric and the two-dimensional plane case; $\alpha = 0.2$, $R_e = 1$. ——, For axisymmetric tube; – – –, for two-dimensional channel.

the work done by the wall to a relatively greater degree than in the large R_e case. It is therefore thought that the efficiency becomes smaller for increasing R_e as a result of this variation in energy exchange.

In figure 11, a comparison between the efficiencies of the axisymmetric case and the two-dimensional plane case (Takabatake *et al.* 1985) is made for several values of ϕ. As ϕ increases, the backward flow at the narrowest region of the tube, which is considered to be a kind of ineffective leakage, becomes small, and, in addition, the fluid transport can be performed effectively due to the appearance of trapping. Hence, the pumping efficiency increases remarkably. From the results of figure 11 it may be concluded that the efficiency in a tubular configuration is much higher than that in a two-dimensional plane configuration for all values of ϕ. This is in contrast to the results of Shapiro *et al.*

4. Concluding remarks

A finite-difference technique employing the upwind SOR method has been adopted for the study of axisymmetric peristaltic flows. The influences of the magnitudes of the wave amplitude, the wavelength, and the Reynolds number on the flow are investigated through numerical calculations over a wide range of these quantities. A quantitative comparison is also made between the results for the axisymmetric tube and the two-dimensional plane channel.

The nature of the reflux phenomenon in axisymmetric flow depends upon the Reynolds number as well as the wavenumber. That is, the reflux is found near the axis of the tube at large Reynolds number and/or at large wavenumber, while it occurs near the tube wall when both Reynolds number and wavenumber are small. This feature is qualitatively similar to that obtained in two-dimensional flow by the authors. But the fluid mixing that results from peristaltic reflux is much stronger for the case of circular cylindrical tubes than for two-dimensional channels. The

contribution of the trapping to fluid transport is much greater in cylindrical geometry. As a result, the pumping efficiency is also greater for cylindrical tubes than for two-dimensional plane channels. It is evident from these facts that the mixing and transport mechanisms in peristalsis are more effective in a cylindrical tubular configuration than in a plane configuration.

This work was partially supported by a Grant-in-Aid for Scientific Research from the Ministry of Education (Japan).

Appendix A. A finite-difference method

Here we set out finite-difference expressions for the axisymmetric case. The following expressions are derived from the governing equations:

$$a_0\psi_{i,j}+a_1\psi_{i+1,j}+a_2\psi_{i,j+1}+a_3\psi_{i-1,j}+a_4\psi_{i,j-1}+a_5\psi_{i-1,j-1}+\zeta_{i,j}=0, \tag{A 1}$$

$$b_0\zeta_{i,j}+b_1\zeta_{i+1,j}+b_2\zeta_{i,j+1}+b_3\zeta_{i-1,j}+b_4\zeta_{i,j-1}+b_5\zeta_{i-1,j-1}=0, \tag{A 2}$$

where

$$\left.\begin{aligned} a_0&=-\frac{2}{h_i^2}-\frac{\alpha^2}{k^2}(2+D_{i,j}), \quad a_1=\frac{\alpha^2}{k^2}, \quad a_2=-\frac{1}{2h_i r_{i,j}}+\frac{1}{h_i^2}+\frac{\alpha^2}{2k^2}(D_{i,j}-2K_{i,j})\\ a_3&=\frac{\alpha^2}{k^2}(1+M_{i,j}), \quad a_4=\frac{1}{2h_i r_{i,j}}+\frac{1}{h_i^2}+\frac{\alpha^2}{2k^2}(D_{i,j}+2K_{i,j}), \quad a_5=-\frac{\alpha^2}{k^2}M_{i,j}, \end{aligned}\right\} \tag{A 3}$$

$$\left.\begin{aligned} b_0&=r_{i,j}a_0+\frac{R_e}{2kh_i}\left\{-|\beta|-|\gamma|+\operatorname{sgn}(\beta)\operatorname{sgn}(\gamma)\tfrac{1}{2}\gamma T_{i,j}-\frac{2h_{i,j}}{r_{i,j}}(\beta-\gamma\tfrac{1}{2}S_{i,j})\right\},\\ b_1&=r_{i,j}a_1+\frac{R_e}{2kh_i}\gamma\{H(\gamma)-1\}, \quad b_2=r_{i,j}a_2+\frac{R_e}{2kh_i}\{|\beta|-\operatorname{sgn}(\beta)\operatorname{sgn}(\gamma)\tfrac{1}{2}\gamma T_{i,j}\}H(\beta),\\ b_3&=r_{i,j}a_3+\frac{R_e}{2kh_i}\gamma H(\gamma), \quad b_4=r_{i,j}a_4+\frac{R_e}{2kh_i}\{|\beta|-\operatorname{sgn}(\beta)\operatorname{sgn}(\gamma)\tfrac{1}{2}\gamma T_{i,j}\}\{1-H(\beta)\},\\ b_5&=r_{i,j}a_5, \end{aligned}\right\} \tag{A 4}$$

and $D_{i,j}$, $K_{i,j}$, $M_{i,j}$, $S_{i,j}$, $T_{i,j}$, β, γ, $H(x)$ and $\operatorname{sgn}(x)$ are defined as in T & A.

The difference approximations to ζ at the boundary are as follows:

$$\left.\begin{aligned} &\zeta_{i,j}=0 \quad \text{(at the centre axis)},\\ &\zeta_{i,j}=d_{0j}\psi_{i,j}+d_{1j}\psi_{i-1,j}+d_{2j}\psi_{i-2,j}+d_{3j}\psi_{i,j+1}+d_{4j}\psi_{i,j-1} \quad \text{(at the leading end)},\\ &\zeta_{i,j}=e_{0i}\psi_{i,j-1}+e_{1i}\psi_{i-1,j-1}+e_{2i}(\tfrac{1}{2}q)+e_{3i}r_{i,j} \quad \text{(at the wall)},\\ &\zeta_{i,j}=d_{0j}\psi_{i,j}+d_{1j}\psi_{i+1,j}+d_{2j}\psi_{i+2,j}+d_{3j}\psi_{i,j+1}+d_{4j}\psi_{i,j-1} \quad \text{(at the trailing end)},\\ &\zeta_{i,j}=f_0\psi_{i,j-1}+f_1\psi_{i-1,j-1}+f_2(\tfrac{1}{2}q)+f_3r_{i,j} \quad \text{(at the wall point on the leading end)},\\ &\zeta_{i,j}=f_0\psi_{i,j-1}+f_1\psi_{i+1,j-1}+f_2(\tfrac{1}{2}q)+f_3r_{i,j} \quad \text{(at the wall point on the trailing end)}, \end{aligned}\right\} \tag{A 5}$$

where

$$
\left.\begin{aligned}
&d_{0j}=\frac{2}{h_1^2}+\frac{\alpha^2}{k^2}\left(\frac{S_{2,j}+K_{2,j}}{T_{2,j}}+K_{1,j}M_{2,j}\right),\quad d_{1j}=-\frac{2\alpha^2}{k^2}\frac{S_{2,j}}{T_{2,j}},\quad d_{2j}=\frac{\alpha^2}{k^2}\frac{h_1}{h_2}\frac{K_{1,j}}{T_{2,j}},\\
&d_{3j}=\frac{1}{2h_1 r_{1,j}}-\frac{1}{h_1^2}-\frac{\alpha^2}{2k^2}K_{1,j}M_{2,j}\left(1-\frac{h_1}{h_2}\frac{1}{T_{2,j}}\right),\\
&d_{4j}=-\frac{1}{2h_1 r_{1,j}}-\frac{1}{h_1^2}-\frac{\alpha^2}{2k^2}K_{1,j}M_{2,j}\left(1+\frac{h_1}{h_2}\frac{1}{T_{2,j}}\right),\\
&e_{0i}=-\frac{2}{h_i^2}-\frac{\alpha^2}{k^2}D_{i,M+1},\quad e_{1i}=\frac{\alpha^2}{k^2}M_{i,M+1},\\
&e_{2i}=\frac{2}{h_i^2}+\frac{\alpha^2}{k^2}(D_{i,M+1}-M_{i,M+1}),\quad e_{3i}=-\frac{1}{r_{i,M+1}}+\frac{2}{h_i}-\frac{\alpha^2}{k^2}(2\delta_{i,M+1}-h_i D_{i,M+1}),\\
&f_0=-\frac{2}{h_1^2}-\frac{2\alpha^2}{k^2}K_{1,M+1}\left(K_{1,M+1}-\frac{h_2}{h_1}\right),\quad f_1=-\frac{2\alpha^2}{k^2}\frac{h_1}{h_2}K_{1,M+1},\\
&f_2=\frac{2}{h_1^2}+\frac{2\alpha^2}{k^2}k_{1,M+1}\left(K_{1,M+1}-\frac{h_2}{h_1}+\frac{h_1}{h_2}\right),\\
&f_3=-\frac{1}{r_{1,M+1}}+\frac{2}{h_1}+\frac{2\alpha^2}{k^2}K_{1,M+1}(h_1K_{1,M+1}-h_2).
\end{aligned}\right\}\qquad (A\ 6)
$$

Finally, the following expressions for ψ at the interior points next to the boundary are obtained from the boundary conditions:

$$
\left.\begin{aligned}
&\psi_{i,j}=\tfrac{1}{4}\psi_{i,j+1}\quad\text{(at the centre axis)},\\
&\psi_{i,j}=\frac{\delta_{i-1,j}\psi_{i+1,j}+\delta_{i,j}\psi_{i-1,j}}{\delta_{i,j}+\delta_{i-1,j}}\quad\text{(at the leading end)},\\
&\psi_{i,j}=\tfrac{1}{4}(\psi_{i,j-1}+\tfrac{3}{2}q+2h_i r_{i,j+1})\quad\text{(at the wall)},\\
&\psi_{i,j}=\frac{\delta_{i,j}\psi_{i-1,j}+\delta_{i-1,j}\psi_{i+1,j}}{\delta_{i,j}+\delta_{i-1,j}}\quad\text{(at the trailing end)}.
\end{aligned}\right\}\qquad (A\ 7)
$$

Appendix B. Pumping efficiency in the linear theory

We consider the limiting case, $R_e\to 0$, $\alpha\to 0$, which is identical with the situation considered by Shapiro *et al.* (1969). In the denominator of the efficiency expression, (8), the contributions of σ_r and τ_{zr} are negligible for the case of $\alpha\to 0$. Neglecting these terms, the denominator is given as

$$
W_L=-\frac{1}{T_w}\int_0^{T_w}\int_0^{\lambda}2\pi Hvp\,\mathrm{d}Z\,\mathrm{d}T. \qquad (B\ 1)
$$

Substituting v and p from the linear solutions of Shapiro *et al.* and H from the definition for the wall motion, we finally obtain

$$
\begin{aligned}
W_L=\frac{2\pi\mu c^2\lambda}{(1-\phi^2)^{\frac{7}{2}}}\Bigg[&-\frac{\phi^4(16-\phi^2)^2}{4+6\phi^2}\left(\frac{\bar{Q}}{\bar{Q}_{\max}}\right)+4+4(1-\phi^2)^{\frac{7}{2}}+10\phi^2\\
&+7\phi^4+\tfrac{3}{2}\phi^6-8(1+\tfrac{1}{2}\phi^2)(1-\phi^2)^2\Bigg]. \qquad (B\ 2)
\end{aligned}
$$

The last term in the brackets of (B 2) is missing in the final expression obtained by Shapiro *et al.*, that is, equations (31*a*) and (31*b*) in their paper.

If we consider $\phi = 0$ and $\bar{Q}/\bar{Q}_{\max} = 0$, W_L of (B 2) will vanish, whereas W_L by Shapiro *et al.* will not become zero because this term is missing. Physically, this assumption means that the fluid is stationary in the absence of wall motion, hence W_L should inevitably vanish.

REFERENCES

AYUKAWA, K., KAWAI, T. & KIMURA, M. 1981 Streamlines and path lines in peristaltic flows at high Reynolds numbers. *Bull. Japan Soc. Mech. Engrs* **24**, 948–955.

AYUKAWA, K. & TAKABATAKE, S. 1982 Numerical analysis of two-dimensional peristaltic flows (1st report; flow pattern). *Bull. Japan Soc. Mech. Engrs* **25**, 1061–1069.

BÖHME, G. & FRIEDRICH, R. 1983 Peristaltic flow of viscoelastic liquids. *J. Fluid Mech.* **128**, 109–122.

BRASSEUR, J. G., CORRSIN, S. & LU, N. Q. 1987 The influence of a peripheral layer of different viscosity on peristaltic pumping with Newtonian fluids. *J. Fluid Mech.* **174**, 495–519.

BROWN, T. D. & HUNG, T.-K. 1977 Computational and experimental investigations of two-dimensional nonlinear peristaltic flows. *J. Fluid Mech.* **83**, 249–272.

FUNG, Y. C. & YIH, C. S. 1968 Peristaltic transport. *Trans. ASME* E: *J. Appl. Mech.* **35**, 669–675.

GREENSPAN, D. 1968 *Lectures on the Numerical Solution of Linear, Singular, and Nonlinear Differential Equations*, pp. 122–147. Practice-Hall.

GUPTA, B. B. & SESHADRI, V. 1976 Peristaltic pumping in non-uniform tubes. *J. Biomech.* **9**, 105–109.

HANIN, M. 1968 The flow through a channel due to transversely oscillating walls. *Israel J. Tech.* **6**, 67–71.

JAFFRIN, M. Y. 1973 Inertia and streamline curvature effects on peristaltic pumping. *Intl J. Engng Sci.* **11**, 681–699.

JAFFRIN, M. Y. & SHAPIRO, A. H. 1971 Peristaltic pumping. *Ann. Rev. Fluid Mech.* **3**, 13–36.

LI, C. H. 1970 Peristaltic transport in circular cylindrical tubes. *J. Biomech.* **3**, 513–523.

LIRON, N. 1976 On peristaltic flow and its efficiency. *Bull. Math. Biol.* **38**, 573–596.

LONGUET-HIGGINS, M. S. 1983 Peristaltic pumping in water waves. *J. Fluid Mech.* **137**, 393–407.

MANTON, M. J. 1975 Long-wavelength peristaltic pumping at low Reynolds number. *J. Fluid Mech.* **68**, 467–476.

POZRIKIDIS, C. 1987 A study of peristaltic flow. *J. Fluid Mech.* **180**, 515–527.

RATH, H. J. 1978 Ein Beitrag zur Berechnung einer peristaltischen Strömung in elastischen Leitungen. *Acta Mech.* **31**, 1–12.

SHAPIRO, A. H., JAFFRIN, M. Y. & WEINBERG, S. L. 1969 Peristaltic pumping with long wavelengths at low Reynolds number. *J. Fluid Mech.* **37**, 799–825.

SRIVASTAVA, L. M. & SRIVASTAVA, V. P. 1984 Peristaltic transport of blood: Casson model II. *J. Biomech.* **17**, 821–829.

STOKES, G. G. 1847 On the theory of oscillatory waves. *Trans. Camb. Phil. Soc.* **8**, 441–455.

TAKABATAKE, S. & AYUKAWA, K. 1982 Numerical study of two-dimensional peristaltic flows. *J. Fluid Mech.* **122**, 439–465.

TAKABATAKE, S., AYUKAWA, K. & OKURA, M. 1985 Numerical analysis of two-dimensional peristaltic flows (3rd report; pumping characteristics of peristaltic transport). *Trans. Japan Soc. Mech. Engrs* **51**, 2365–2372 (in Japanese).

TONG, P. & VAWTER, D. 1972 An analysis of peristaltic pumping. *Trans. ASME* E: *J. Appl. Mech.* **39**, 857–862.

YIN, F. & FUNG, Y. C. 1969 Peristaltic waves in circular cylindrical tubes. *Trans. ASME* E: *J. Appl. Mech.* **36**, 579–587.

ZIEN, T. F. & OSTRACH, S. 1970 A long wave approximation to peristaltic motion. *J. Biomech.* **3**, 63–75.